Carbon Nanotube-Based Wearable Sweat Sensors; Design and Fabrication

Vigneshwar Sakthivelpathi

A thesis

submitted in partial fulfilment of the

requirements for the degree of

Master of Science in Mechanical Engineering

University of Washington

2019

Committee:

Jae-Hyun Chung

Nathan Sniadecki

Ji-Eun Kim

Program Authorized to Offer Degree:

Mechanical Engineering

University of Washington

Abstract

Carbon Nanotube-Based Wearable Sweat Sensors; Design and Fabrication

Vigneshwar Sakthivelpathi

Chair of the Supervisory Committee:

Jae-Hyun Chung

Department of Mechanical Engineering

Wearable sweat sensors enable non-invasive diagnosis of various diseases and real-time health monitoring. Few sensors exhibit pH measurement on skin due to interference by sodium chloride ions. This thesis presents a multiplexing wearable sweat sensor using single and multi-walled carbon nanotubes. The wearable device houses pH, humidity, temperature and sodium chloride sensors. The potential change of a pH sensor is calibrated by measuring sodium chloride ion concentration with resistance. Each sensor's response is studied in terms of resistance or potential change. Sensor accuracy, sensitivity and usability is tested through a simulated sweat experiment, where the sensing parameters are measured in real-time. This multiplexing sweat sensor provides an accurate, low-cost, integrated platform to monitor multiple physiological parameters in sweat.

University of Washington

Graduate School

2019

This is to certify that I have examined this copy of a master's thesis by

Vigneshwar Sakthivelpathi

and have found that it is complete and satisfactory in all respects,

and that any and all revisions required by the final

examining committee have been made.

Reading Committee:

_____

Associate Professor Jae-Hyun Chung, Chair

_____

Associate Professor Nathan Sniadecki

_____

Assistant Professor Ji-Eun Kim

Date: _____

In presenting this thesis in partial fulfillment of the requirements for a master's degree at the University of Washington, I agree that the Library shall make its copies freely available for inspection. I further agree that extensive copying of the thesis is allowable only for scholarly purposes, consistent with "fair use" as prescribed in the U.S. Copyright Law. Any other reproduction for any purposes or by any means shall not be allowed without my written permission.

_____

Vigneshwar Sakthivelpathi

Date: _____

TABLE OF CONTENTS

LIST OF FIGURES

LIST OF TABLES

ACKNOWLEDGEMENTS

I wish to express my gratitude to Professor Jae-Hyun Chung for his ongoing encouragement, valued advice, support and trust in my abilities.

And to the members of The Nanomanufacturing Laboratory, Seong Kahng, Jinyuan Zhang and Wenqing Ju for their ongoing support.

DEDICATION

I dedicate this dissertation to my father, Dr Sakthivelpathi Sarangapani and mother, Karpagam Sakthivelpathi. For my successes are built on their sacrifice, determination and love.

Chapter 1. INTRODUCTION

1.1 WEARABLE BIOSENSORS

A biosensor can be defined as a self-contained integrated device that can provide quantitative or qualitative information using a biological recognition element [1]. It comprises of three main elements; a biological receptor (sample), transducer (sensing element) and signal processor (data analyzer). With the rapid development of microprocessor chips and micro / nanoscale fabrication methods, traditional biosensors have evolved to a thin-film. Advancements in manufacturing and packaging technologies have enabled the integration of microelectronic and micromechanical sensors into minuscule rigid or flexible substrates with high sensitivity and low cost [2]. The advancement coupled with interchanging desktop processors with mobile technologies (i.e. smartphones, tablets etc.) has allowed wearable biosensors to challenge the arena of affordable healthcare, enabling point-of-care monitoring, and non-invasive analysis of an individual's vital physiological elements [2]. Heart rate monitors, sleep monitors, fitness trackers and smart glasses are examples of a multitude of sensory devices that can be classified as a form of wearable biosensor devices. A key indicator of growth in wearable biosensors is the expansion of the global market for wearable medical devices, with BBC Research suggesting a $8.9 billion market share in 2018 rising to $29.9 billion by 2023 [3].

Though chipset and microprocessor advancements have aided in the development of the wearable biosensor, the quintessential element in reducing scale and increasing accuracy has been the advent of nanostructured manufacturing. A nanostructure is an

object that has at least one dimension equal to or smaller than 100 nanometers (nm) [4]. There are various nanostructures such as; nanoparticles, nanopores, nanorods, nanowires, nanoribbons, nanotubes. Carbon-based nanostructures display unique properties and morphological flexibility, which is characteristically multifunctional and compatible with detecting variations in organic and inorganic systems [5]. Specifically, carbon nanotubes (CNT) have aspect ratios in the order of thousands, which renders high specificity and sensitivity. The molecular dimension is ideal for low power operation for a wide range of electrochemical biosensors [5], [6].

Wearable biosensors have further enabled non-invasive access to screening physiological elements of human body that were previously deemed extremely challenging and expensive for analysis via traditional sensor technologies. Sweat, saliva and tears are non-invasive biological fluids that contain multiple physiologically relevant chemical constituents, which can be readily used to monitor human health and performance in real-time [7]. Analyzing the patterns of the chemical elements within sweat can aid in the identification of many physiological diseases and disorders. In particular, the sensors can reveal therapeutic information such as an athlete's electrolytic losses, biological pH level Diseases like Alzheimer's and cystic fibrosis can be detected in such biological samples [8]–[11]. In the last decade, sweat analysis study has rapidly blossomed with a wearable platform to enable real-time, prolonged monitoring. The high sensing performance equivalent to laboratory equipment could replace the bulky equipment required for laboratory-based sample collection and processing.

1.2 SWEAT BIOLOGY

Health monitoring is typically conducted by analyzing a bodily fluid. Blood is a commonly used fluid due to rich physiological and biological information. Blood collection requires an invasive extraction method and rigorous testing within a lab-based environment, which does not allow for real-time, point-of-care monitoring. Human sweat is abundant with biological information and can enable non-invasive, continuous monitoring of an individual's health state [12]. The human body contains 1.6 to 5 million eccrine, apocrine and apoeccrine sweat glands, distributed over the whole body, with an average density of 200 sweat glands/cm^2. Sweating can occur due to;

- Thermoregulatory – temperature reduction under heat stress conditions [10].
- Emotions – physical reaction to emotive stimuli like stress, anxiety, fear and pain that is most evident on palms, soles and in the axillary region [10].
- Gustatory irregularity – ingestion causing an increase in metabolism, leading to elevated body temperature and thermal sweating [10].

Sweat contains elements such as sodium (Na^+), chloride (Cl^-), potassium (K^+), magnesium (Mg^{2+}), calcium (Ca^{2+}), lactate, ammonium, and acts as a pH level indicator [13]. The analysis of sodium chloride (NaCl) and pH is key to this research, as various human health and behavior issues can be evaluated. Sodium chloride concentrations increase in patients with cystic fibrosis (CF), Alzheimer's disease (AD), diabetes insipidus, hypothyroidism and adrenal insufficiency [8], [11]. CF is a genetic disease where a defective gene leads to the creation of thicker, sticker mucus. Lung infections are caused by accumulation mucus in the lung. Mutations in the cystic fibrosis transmembrane conductance regulator (CFTR) gene, abundantly expressed in the human

re-absorptive duct, cause irregularities in ductal electrolyte reabsorption leading to increased sweat chloride levels [10]. Hall et al., tested sweat sodium and chloride ranges in adults with chest disease and CF utilizing pilocarpine iontophoresis;

Table 1.1. Sodium and chloride concentration range in sweat for adults [11].

	Normal Adult	**Chest Disease**	**CF**
Na range (mM)	29-72	29-77	84-137
Cl range (mM)	14-48	13-52	81-122

AD is a debilitating progressive illness that destroys an individual's memory and mental function. Although incurable, progression can be slowed, especially with early detection. A clinical study of 44 women by Elmstähl et al., reported an increase in sweat osmolality, with AD patients showing a mean sodium concentration of 91 ±41 mM, which was substantially higher than the 62 ±29 mM observed in patients without AD [8].

Table 1.2. Sweat gland density by body region, through direct counting technique [10].

Region	**Sweat Gland Density (glands per cm^2)**
Palms	644
Forearm	134
Abdomen	127
Upper arm	90
Armpit	68
Thigh	57
Face	59
Chest	20

Aside from analyzing the chemical elements within sweat, the ability to track its acidity levels enables correlation to several health factors. Changes in sweat pH have been reported to play a role in the pathogenesis of skin diseases (like irritant contact dermatitis and acne), detecting conditions, such as metabolic alkalosis. Traditionally, electrochemical sensors with glass ion selective membranes are used to detect pH levels. Miniaturizing these sensors has been difficult, as reference electrodes are bulky and without ion selective membranes accuracy is lost [14]. Physiological metrics like sweat rate and dehydration are indicators in sweat for health conditions [15]. Patterson et al. reported relationships between sweat NaCl and the acid-base status of the sweat. As the sweat NaCl was reduced, the sweat pH level also decreased [15], [16]. Furthermore, as exercise in a dehydrated condition has been shown to lead to increased levels of Na^+, sweat pH can therefore be a direct indicator for dehydration levels during any physical

activities [15], [16]. Rahimi et al. described a pH sensors ability to remotely analyses the state of a healing wound. Healthy skin has slightly acidic pH (5.5–6.5), but infected chronic wounds often exhibit pH values higher than 7.4, due to the alkaline by-products of proliferating bacterial colonies [17]. Fig. 1.1 shows the accuracy and repeatability of the solid-state pH sensor developed by Rahimi et al. The sensor utilizes carbon electrodes with a polyaniline sensing tip and Ag/AgCl reference electrode.

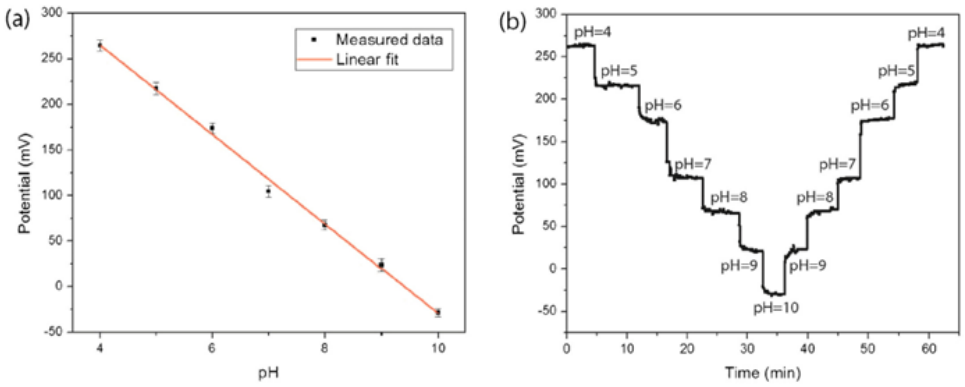

Fig. 1.1. (a) Measured sensor response to pH levels between 4 and 10. (b) Sensor response to increasing and decreasing pH solutions from pH 4 to pH 10 [17].

1.3 Key Metrics and Physiological Range

Sweat is composed of a multitude of chemical elements, each capable of contributing vital physiological information with respect to any bodily change or dysfunction. A biosensor which can monitor each of these elements in real time would be ideal, but not practical. Therefore, it is important to identify which elements are easily detectable and capable of providing relevant information to health conditions. Sweat contains a sodium composition of up to 0.863 ± 0.563 g/L [18]. Along with chloride, sodium is the most abundant ion in sweat, playing a role in indicating general health vitality and detecting diseases such as Alzheimer's and cystic fibrosis. The clinically

important NaCl concentrations will include levels during normal human functionality, AD and CF [11], [13], [19], [20]. In sweat, pH is often considered an index of hydration rate [19] and a progression indicator of skin diseases. Furthermore, pH changes correlate with deviations in NaCl, subsequently enabling cross-verification between metrics. The experimental range will include levels during normal human functionality and strenuous exercise [13], [19], [20]. Skin temperature and humidity will also be measured as general physiological metrics related with health dysfunction and sweat rate. Temperature range will be between normal functionality and hyperpyrexia [21].

Table 1.3. Physiological elements and their respective experimental detection range.

Physiological Elements	**Range in Humans**
NaCl	10 to 140 mM
pH	5 to 7
Temperature	36.5 to 42^{o}C
Humidity	0 to 100%

Chapter 2. LITERATURE REVIEW

2.1 CARBON NANOTUBE SENSORS – SINGLE AND MULTI-WALLED

Carbon is one the most abundant and versatile elements on earth. Depending on the atomic structure and bonding nature, various properties can be created [22]. Fullerenes are carbon allotropes with molecules composed entirely of carbon and in the form of hollow spheres or tubes. The cylindrical fullerenes are known as carbon nanotubes (CNT). They have a very similar structure to graphene, with the atoms arranged in a hexagonal lattice and nanometer sized in diameter and length, with the length to diameter ratio exceeding 1000 [22]. CNTs are formed by rolling a sheet of graphene into a cylindrical shape, as shown in Fig. 2.1. Different types of CNTs with unique physical properties can be created by varying the way in which the graphene sheets are rolled.

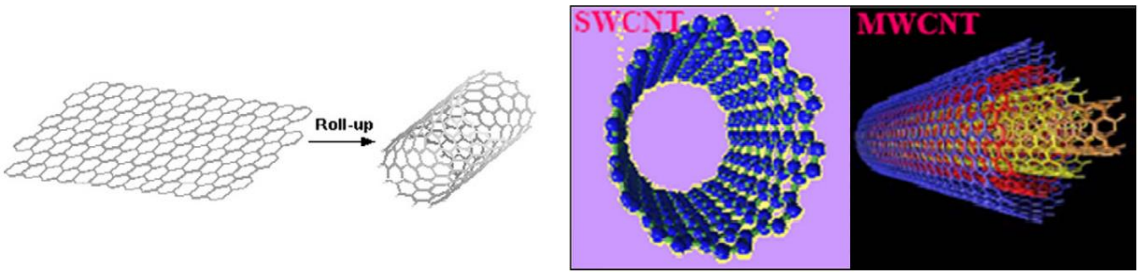

(a) (b)

Fig. 2.1. (a) Graphene sheet rolled into a CNT. (b) Structure of SWCNT and MWCNT [22].

CNTs have outstanding physical properties including; high strength, stiffness and hardness, but the key property that enables their functionality across multiple platforms is their high thermal and electrical conductivity. This high conductivity is a consequence of

the atomic bonding structure of carbon atoms. A carbon atom has six electrons in a $1s^2 2s^2 2p^2$ shell configuration, with the core electrons (within the $1s^2$ shell) strongly bound to the nucleus and the remaining ($2s^2 2p^2$) valence electrons bound weakly [23]. These valence electrons rehybridize to form more energetically favorable bonds with adjacent atoms. In graphene, a particular type of rehybridization occurs where a sheet of carbon atoms arrange in a hexagonal lattice with a basis of two atoms. These valence electrons rehybridize into three sp^2 hybrids and a fourth p_z orbital (see Fig. 2.2). The three sp^2 electrons each form a sigma covalent bond with the three neighboring carbon atoms 120° apart [23]. The p_z electron exists in in the pi orbital, orthogonal to the sigma covalent bonded electrons. Thus, it is these delocalized pi orbital electrons that enable a CNTs excellent thermal and electrical conductivity.

Groups	Hybridization
1	s
2	sp^1
3	sp^2
4	sp^3
5	sp^3d^1

(a)

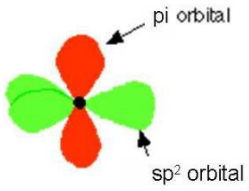

(b)

Fig. 2.2. (a) Atomic orbital hybridization groups. (b) Carbons atoms rehybridizing to form three sp^2 orbitals 120° apart and p_z orbital [23].

CNTs can be primarily split into two types; single walled carbon nanotubes (SWCNT) and multi walled carbon nanotubes (MWCNT). SWCNTs are formed by rolling a single layer of graphene into a seamless cylinder. The one-dimensional structure (length to diameter ratio over 1000) has diameters close to 1nm. The method of rolling can produce three distinct lattice structures (see Fig. 2.3); zig zag, arm chair and chiral tubes. Electrical conductivity varies according to the chirality. SWCNTs are divided into

semiconducting and metallic tubes while MWCNTs are metallic [6], [22]. MWCNTs can be considered as a collection of concentric SWCNTs with larger diameters. Their lengths and diameters (>10 nm) vary significantly from SWCNTs with lower synthesis cost [22]. CNTs are typically synthesized via three main methods; arc discharge, laser ablation, and chemical vapor deposition [22].

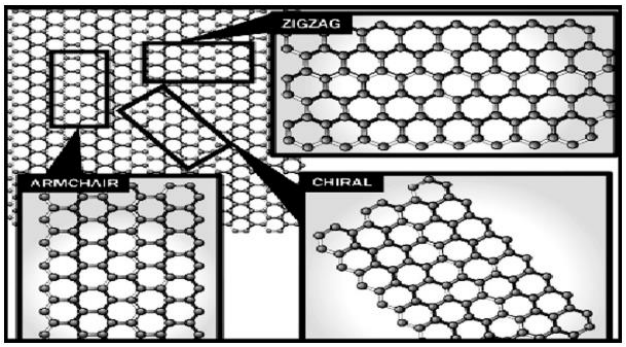

Fig. 2.3. Differing carbon nanotube chirality structures [22].

2.2 THEORETICAL WORKING PRINCIPLE

2.2.1 *pH Sensor*

A pH sensor works by using an 'ion transducer' to measure the acidity of a sample solution (sweat) by detecting the potential change between two dissimilar electrodes. The cathode consists of SWCNTs coated with polyaniline on a gold electrode, while the anode is made up of a silver electrode covered with a silver chloride (AgCl) sensing tip (refer to section 4.1 Sensor Fabrication for further details). When in contact with the sample fluid, the anode undergoes a redox reaction as per Eqn. 2.1. The cathode experiences an entirely different chemical reaction whereby the carbon nanotubes act as an ion transducer to convert proton ion (H^+) concentration into electrons.

$$AgCl(s) + e^- \rightleftharpoons Ag(s) + Cl^-(aq) E^o \approx 0.222V \quad (2.1)$$

As detailed in section 2.1 Carbon Nanotube Sensors, the bonding structure of a semiconducting SWCNT provides a delocalized electron at every node within the lattice structure. These delocalized electrons of SWCNTs weakly bind with oxygen and nitrogen in air, which makes SWCNTs as a p-type. When in contact with a sample fluid, the electrons surrounding the SWCNT attract the abundant H^+ ions, which alter the potential charge at the electrode. This change in potential consequentially impacts the overall cell potential, that is measured between the anode and cathode. Calibrating this cell potential will result in a highly accurate measure of pH level in a liquid sample.

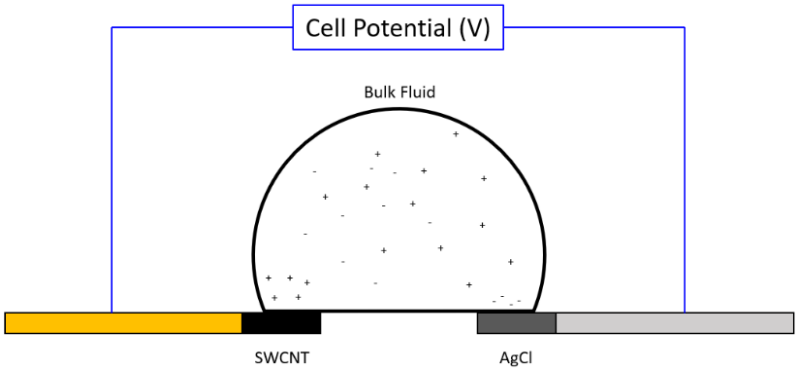

Fig. 2.4. pH ion transducer working principle schematic.

2.2.2 *Humidity Sensor*

A MWCNT humidity sensor is a CNT gas sensor combined with a CNT strain sensor due to cellulose fiber expansion. A humidity sensor is a carbon nanotube paper composite (CPC), that is fabricated by immersing tissue paper in a MWCNT solution (refer to section 4.1 Sensor Fabrication for further details). The CNTs present in a CPC are p-type and subsequently binds H^+ ions from disassociated water vapor. The gradual increase of H^+ ions causes a change in the carrier concentration resulting in an almost linear increase in the resistivity of the CPC. However, when relative humidity (RH)

reaches 80%, the CPC resistance change is dominated by swelling of the cellulose fibers, altering the electron transport between conducting CNT networks. The swelling effect causes a steep increase in sensitivity and becomes the dominant mechanism in changing the resistance of the sensor (refer to Fig. 2.5). Calibrating this change in resistivity will result in an accurate measure of the RH.

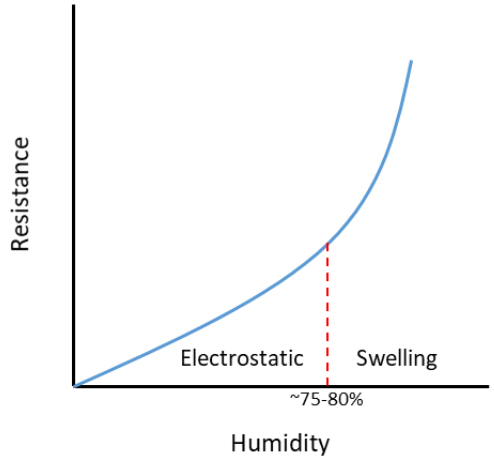

Fig. 2.5. Relationship between resistance and humidity with respect to a CPC sensor.

2.2.3 *Temperature Sensor*

Like the humidity sensor, a temperature sensor is made of a CPC. The electrical conductivity of a polymer composite is governed by the electrically percolated network formed by the CNTs within an electrically insulating polymer matrix [24]. CNTs in polymeric composites are not necessarily in contact but are often separated by small distances (tunneling distance) due to the presence of polymer layers in between. This implies the consideration of the tunneling effect between CNTs as a conduction mechanism, which affects the effective electrical conductivity / thermo-resistivity of the composite material. Under temperature variations, the separation distance between CNTs changes due to thermal expansion, which modifies the electrical conductivity of the

whole composite [24]. Although not polymeric, the MWCNT temperature sensor is a paper composite where interactions between CNTs and cellulose layers behave in a manner similar to polymeric CNT composites. The chirality of CNTs have a considerable effect on the resistive response with respect to change in temperature [24]–[26]. Within the physiological range considered in this research, the change in resistance in the temperature sensor is expected to linearly decrease with an increase in temperature (refer to Fig. 2.6).

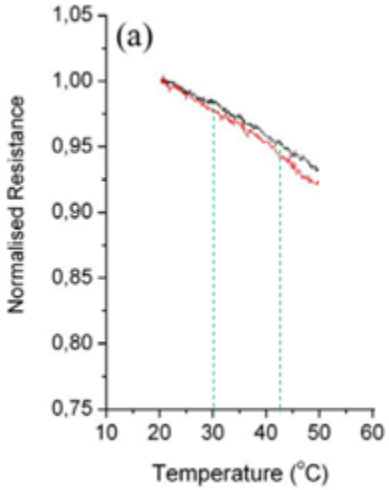

Fig. 2.6. The resistance of two different CNTs normalized at the heating start point [25].

2.2.4 *Sodium Chloride Resistive Sensor*

The sodium chloride resistive sensor is based on the principle that conductivity of a fluid will vary with respect to changes in its ionic concentration. Sweat is a biological fluid that is composed of a multitude of anions and cations, with Na^+ and Cl^- being the most dominant by concentration. Thus, an increase in the dominant ion's concentration (in sweat) will increase the conductivity, and decrease the resistivity. This sensor will use gold nanowire electrodes to apply a known voltage source through the sample fluid to

analyses the change in resistance. The equivalent electrical circuit for the resistive sensor can be modelled as shown in Fig. 2.7. Where C_{dl} is the electrical double layer (EDL) capacitance between the gold electrodes and bulk fluid, C_p is the parasitic capacitance, R_s is the resistance measured by the sensor, and R_{ref} is the ohmic reference resistor. A DC source provides a square wave pulse input. The parasitic- and electrical double layer capacitance can be substantially reduced by decreasing the size of the electrodes.

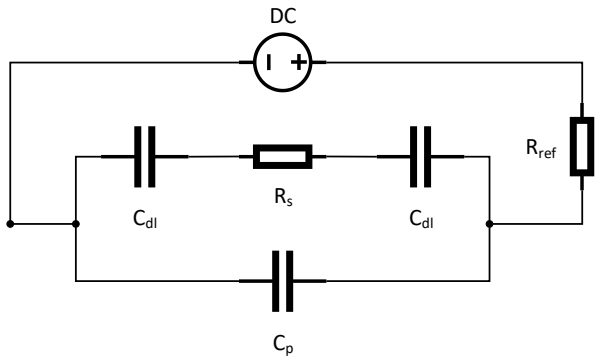

Fig. 2.7. NaCl resistive sensor equivalent circuit.

The parasitic capacitance will remain constant as the surface area of the electrodes or substrate remains the same. The EDL capacitance will vary with the ionic concentration of the fluid. This constant parasitic capacitance and varying EDL capacitance are intrinsically a component of the total impedance value that will be measured from the sensor. This resistance can be regarded as the total impedance of the sensor. Therefore, the resistance of this sensor can be re-written as per Eqn. 2.2, where Z_s is the impedance measured by the sensor. R_{ref} is the Ohmic reference resistor, V_{in} is the input voltage and V_s is the voltage measured across the sensor.

$$Z_s = \frac{R_{ref}}{\left(V_{in}/V_s\right) - 1} \tag{2.2}$$

2.3 CURRENT DEVICES

2.3.1 *Colorimetric Analysis*

Colorimetric analysis visually determines the state or concentration of a chemical element through the reaction with a pre-calibrated chemical dye reagent. Colorimetric devices are of interest in the field of a wearable microfluidic system. The information about physiological elements can be offered instantly. Koh et al. investigated in situ quantitative analysis of sweat utilizing microfluidic device with chromogenic reagents and near field communication (NFC) for data transmission [19]. The device, shown in Fig. 2.8 (a), could instantaneously measure pH, lactate, chloride and glucose concentrations via photographic RGB analysis of the color change to the chromogenic reagents. With an effective working time of 1 to 6 hours of exercise, the device was composed of a multilayer stack of three subsystems; a skin-compatible adhesive layer with micro openings as a sweat inlet, a seal collection of soft microfluidic channels filled with four color responsive materials and a magnetic loop antenna and NFC electronics for interfacing with an external image capture device [19]. Sweat flows (via capillary forces) into the microfluidic inlets to mix with each of the four colorimetric assay reagents and the serpentine channel. A colorimetric change was then observed (within 1 minute) in each of the four quadrants with respect to deviations in pH, lactate, chloride and glucose concentrations. Sweat rate could also be determined by observing the serpentine channel (~50 μl capacity) where the water responsive cobalt (II) chloride changes from deep blue to pale purple with filling of the reservoir [19]. This device

capitalized on NFC schemes to launch image capture on a mobile device, which was compared with pre-calibrated RGB color codes every 5 minutes. A quantitative measure could be conducted on each of the detected elements [19].

Curto et al. reported a colorimetric microfluidic device (refer to Fig. 2.8 (b)), consisting of polymethyl methacrylate and pressure-sensitive adhesive (PSA-AR9808) platform, using CO_2 ablation laser and lamination [15]. The device detected variations in pH by analyzing changes in color of the 'ionogels' (ionic liquids incorporated into polymer gels) housed within the microfluidic channels. The microfluidic platform consisted of four rectangular ionogel reservoirs and an absorbent reservoir. The absorbent reservoir consisted of a wicking pad that continuously supplied sweat to each of the ionogel reservoirs utilizing capillary forces. Accurate pH values were obtained by observing the barcode color variation in comparison to a standard color chart or via image analysis [15], similar to the technique by Koh et al.

Although colorimetric sensors offered size miniaturization and extraordinary flexibility without electric noise. The limitations of these devices inherently lie in the range of chemical reagents that are available for accurate colorimetric analysis, complex fabrication procedures, requirement for a secondary imaging device for quantitative data and lack of real-time monitoring due to unreliable microfluidic channels [15], [19].

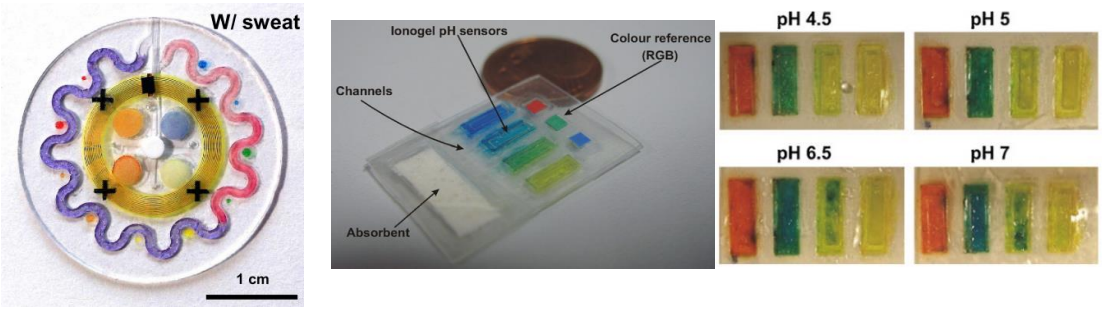

(a) (b)

Fig. 2.8. (a) Koh et al.'s epidermal microfluidic biosensor [19]. (b) Curto et al.'s colorimetric ionogel system tested with artificial sweat [15].

2.3.2 *Electrical Impedance*

Electrical impedance-based sensors use an electrical potential to measure changes in the resistivity of an object. These sensors are particularly effective as they exhibit low power consumption, low cost and a small form factor. Nyein et al. reported a wearable sweat sensing patch that combines an electrical impedance-based sweat rate sensor with a Na^+ ion selective electrode and printed-circuit board (PCB) data analyzer (see Fig. 2.9). The device drew sweat (with capillary action) into a microfluidic channel which housed the ISE and sweat rate electrodes. The Na^+ sensing electrodes were located at the opening of the microfluidic channel, such that ions could be detected as soon as sweat began to accumulate. The sweat rate sensor contained two parallel chromium and gold electrode spirals with a 150 µm, separated by a 100 µm gap [13]. Sweat rate was quantified by measuring the impedance between the two spiral electrodes. As sweat travelled along the channel, the impedance magnitude dropped with increasing sweat volume due to a decrease in the effective resistance and an increase in the capacitance [13]. On-body performance of the sensor was validated with a Marcoduct, a standard sweat collection

apparatus used in CF diagnosis. The sweat rate sensor showed a consistent pattern with results obtained from the Macroduct. Temperature influence on the metal electrodes was shown to be negligible within the relevant physiological range. The device also showed promise in housing extra ISEs to detect other sweat constituents such as K^+, Cl^- and pH.

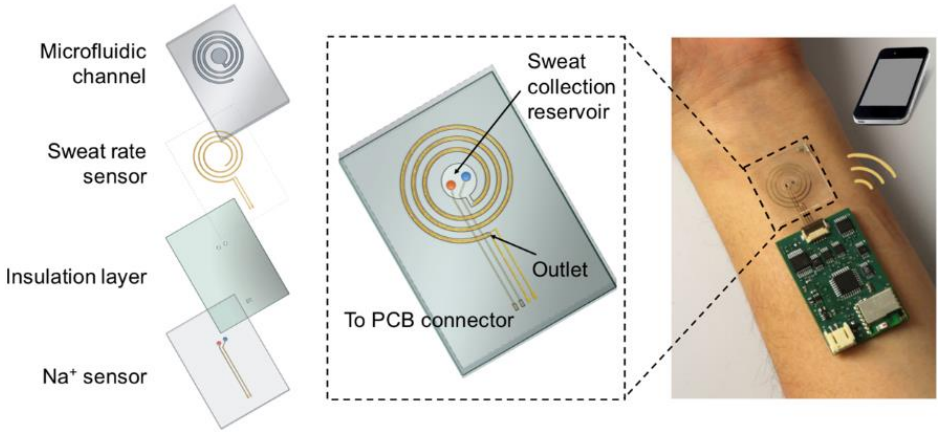

Fig. 2.9. Nyein et al.'s microfluidic sweat rate sensing patch [13].

2.3.3 *Ion Selective Electrode*

The utilization of ion selective electrodes (ISE) in miniaturized electrochemical sensors has proven to be effective in measuring cation and anion concentrations in aqueous based samples, especially sweat. An ISE is a type of electrochemical sensor that converts the activity of a specific ion dissolved in a solution into an electrical potential. An analysis of this potential accurately presents the concentration of the target ion in the solution.

Schazmann et al. investigated an ISE based sodium sensor belt which consolidated sweat collection and analysis in a single device for real-time monitoring of Na^+ ions. The sensor consisted of a hard-plastic platform to fasten the ISEs, a sweat wicking fabric to absorb / pump the sweat to the ISEs sensing tips and a potentiometer for

signal processing. The ISE electrodes were fabricated using PVC tubing as barrels. The reference electrode was filled with 0.1 M potassium chloride (KCl), with the tip plugged with vycor glass to enable ionic interactions. The potentiometric membrane was prepared, and the electrochemical cell was arranged with the following layout; Ag | AgCl | 0.1 M KCl || Sampling Unit | PVC Membrane | 0.1 M NaCl | AgCl | Ag [7]. The wicking patch was constructed using a polyimide-lycra blend. The patch was glued to the plastic platform and pumped fresh sweat from skin to the electrode tips for up to 3 hours (with typical sweat rates). The ISE belt was tested on four healthy and four subjects with CF over 60 minute cycling trials [7]. Atomic absorption spectroscopy was used as the reference method to assess the results from the ISE cycling trial. Results attained were similar but with considerable scatter showing 2~28% deviation between the ISE and reference data. The size and rigidity of the belt meant the device couldn't easily conform to the body's contours, this in turn led to sweat drainage, low sample volume and inadequate contact of ISEs to sweat. Sample volume and proximity of the sensor tips were noted to bear an impact on the detection time and signs of bacterial growth on the vycor reference tips with prolonged use [7].

While Schazmann et al.'s device proved effective in detecting sodium concentrations, the device lacked multiplexing capabilities, and thus was unable to detect other key sweat biomarkers. Gao et al. built on the capabilities of wearable ISEs and reported a device capable of monitoring sodium, glucose, lactate and potassium concentrations in sweat, along with surface skin temperature. The device included signal transduction, conditioning, processing and wireless processing within the wearable format, negating the need for any external potentiometers [12]. The glucose and lactate

sensors were enzymatic and based on glucose oxidase and lactate oxidase immobilized within a permeable film, with Ag / AgCl serving as the electrode material [12]. These enzymatic sensors generated current signals proportional to the abundance of the corresponding metabolites between the working and reference electrode. Sodium and potassium ions were detected via ISE sensors coupled with a polyvinyl butyral (PVB) coated reference electrode, which aided in maintaining potential stability in solutions with varying ionic strengths [12]. A resistance temperature sensor, fabricated using Cr / Au microwires, was also included on the sensor platform. The microcontroller and integrated circuitry were housed on a flexible printed circuit board with the sensors fabricated on a PET substrate.

The device was tested with stationary cycling and outdoor running trials, utilizing the multiplexing sensor as a headband and a wristband. Results attained from the sodium and potassium sensors showed a near Nernstian response, with sensitivities of 64.2 mV and 61.3 mV per decade of concentration, respectively [12]. The results were validated by proving excellent correlation between trial data and ex situ sample analysis (with respect to time). Repeatability tests indicated sensitivity remained constant over a period of four weeks. Real-time temperature compensation was required to ensure the performance of the enzymatic sensors, as they were greatly influenced by any variations. The detection of the chemical elements within sweat was the main focus of this device with monitoring of overall physiological biomarkers such as pH and sweat flow rate ignored. Complex photolithography, O_2 plasma etching and drop casting manufacturing methods were used in fabricating the electrodes and ISEs due to their miniaturized

format. These complex and arduous manufacturing processes were a common theme across wearable ISE electrochemical devices.

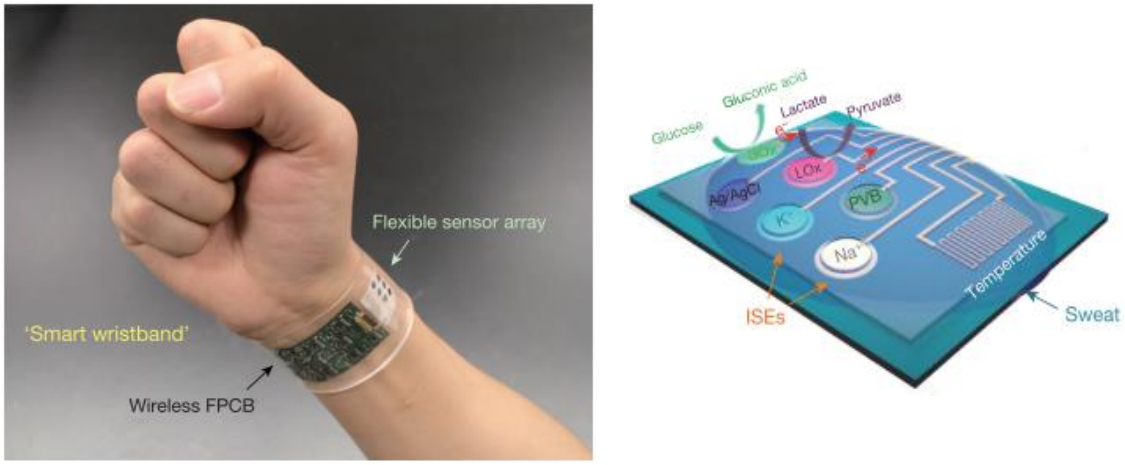

(a) (b)

Fig. 2.10. (a) Gao et al.'s wearable ISE sensor on a subjects wrist [12]. (b) Schematic of Gao et al.'s sensor array [12].

2.3.4 *Salt Bridge*

A challenge in developing wearable potentiometric sensors was that the equilibrium between a reference solution and sample solution could lead to a measurement error over time [27]. Choi et al. reported a novel potentiometric sensor utilizing a salt bridge and silver (Ag) electrodes to accurately measure NaCl concentrations in a sweat sample (refer to Fig. 2.11). The main purpose of a salt bridge was to provide an ionic path between the reference and sample solutions, with respect to the salt bridge geometry. Choi et al.'s prior research created an analytical model to assess the rate of equilibration between reference and sample solutions to predict the measurement error as a function of salt bridge geometry. The sensor was fabricated on a polyethylene terephthalate (PET) film with laser drilling used to define the salt bridge

well and e-beam evaporation to pattern the Ag electrodes. Ag electrodes were patterned on both sides of the PET film with silver chloride (AgCl) ends to act as the reference and sampling electrodes. The salt bridge was created using an agarose gel containing 1 M potassium chloride, covered by an UV curable resin. A potentiometric signal was registered when sample solution met the base AgCl electrodes and created an ionic path through the gelatinous salt bridge [27].

The salt bridge was proven to reduce error and produce stable measurements over prolonged periods. The sensor exhibited small NaCl concentration drift over a 12 hour testing period, with less than 2 mM at 10 mM and 5 mM at 150 mM [27].

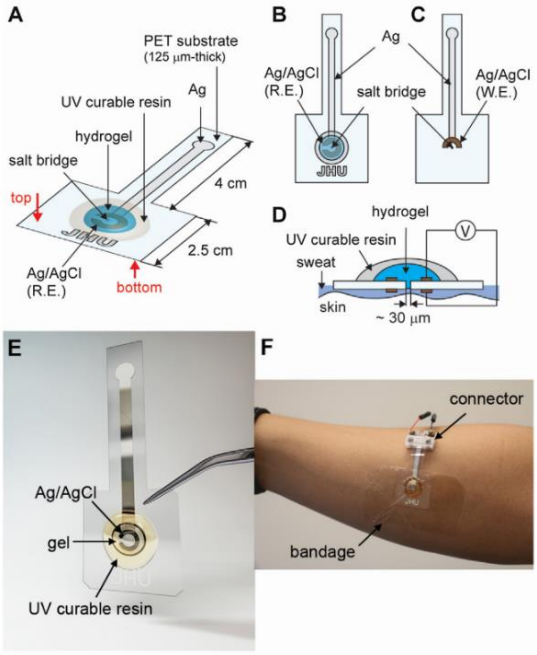

Fig. 2.11. (a) Schematic of the sensor. (b) Top reference side. (c) Bottom sample. (d) Cross-sectional view. (e) Fabricated sensor. (f) Sensor attached to forearm [27].

2.4 CURRENT TESTING METHODOLOGIES

Current testing methodologies included two distinct formats; sweat simulation testing under laboratory conditions and real time human subject testing during exercise. These testing methods were complimentary as one methodology aided in verifying the other. Gao et al.'s ISE sensor accuracy was verified through comparison between on-body sensor readings from the subject with ex situ (off-body) measurements from collected sweat samples [12]. The ex situ sweat was collected by scratching the subject's forehead with microtubes and subsequently tested on a controlled format of the ISE sweat sensor. Real time human subject trials were undertaken during cycling and running, with the subjects wearing the ISE sensors on their wrists and forehead. A moisture absorbent rayon pad was placed between the skin and the sensor array during on-body measurement to maintain adequate sweat volumes and prevent direct contact between the sensors and skin [12]. The newly generated sweat refilled the pad and eliminated the old sweat, maintained real-time sweat flow. The real-time study was conducted as three trials; constant workload cycling, graded workload cycling and outdoor running. Subjects exercised until volitional fatigue at a self-selected pace [12].

Koh et al. used a similar approach to Gao et al. in testing the microfluidic colorimetric sensor. The functionality of the microfluidic channel was tested by comparing the input volume from a syringe pump with the harvested volume in the channel. Indoor and outdoor human trials were conducted to determine the feasibility of using the device under controlled and uncontrolled environmental conditions [19]. The indoor trials included moderate exercise with monitored temperature, humidity, and time. The outdoor trials involved analysis during a 104 km bike race with the colorimetric

sensor placed on the lower back and arm. Image data was obtained periodically with a smartphone. The performance of the device was evaluated by comparing laboratory spectrophotometry analyses to real time human trails. The samples for the laboratory analyses were gathered from absorbing pads applied onto the skin near the sensing region [19].

The electrical impedance based sweat sensor developed by Nyein et al. was characterized in a solution containing NaCl concentration of 15 and 60 mM, which were relevant to the physiological range of sweat Na^+ concentration in humans. To validate on-body performance the Macroduct system was utilized, which is a standard sweat collection system used to diagnose CF. The Macroduct sweat sensing patch was worn alongside the impedance sweat sensor during cycling under a constant power load. The sweat rate patterns and volumes were compared and validated the functionality of the impedance sensor.

Chapter 3. RESEARCH OBJECTIVE

Previous wearable sweat sensor designs had either; addressed the detection of only one physiological element, multiplexed detection only with respect to the chemical constituents in sweat or unable to house the transducer and data analyzer into a wearable format. The objective of this research;

1. is to develop a multiplexing wearable sweat sensor using single and multi-walled carbon nanotubes, while negating the need for complex manufacturing techniques.
2. to study the potential difference of a pH sensor with respect to varying NaCl concentrations, and investigate an approach to compensate the potential changed by NaCl concentration.

The device will integrate the sensors of pH, sodium chloride, temperature and humidity. Both chemical and general physiological elements are detected in simulated human sweat samples. The sensitivity, repeatability and manufacturability will be characterized for each of the four sensors. Important technological barriers such as miniaturization, low cost production, reusability or disposability, robustness, flexibility and adaptability will be addressed through the design of this device. The fabricated sensor will be tested for a simulated sweat setup consisting of wet tissue on a hot plate.

Chapter 4. DESIGN AND EXPERIMENTAL METHOD

4.1 SENSOR FABRICATION

4.1.1 *pH Sensor*

Gold electrodes were printed on a PET film via sputter deposition, with a 5 mm electrode spacing. A thin layer of silver paste was added over one of the electrodes ends (covering approximately $1/5^{th}$ of its length) and baked for 10 minutes over a hotplate at 85^{o}C. Polydimethylsiloxane (PDMS, Sylgard 184 silicone elastomer, Dow Corning Corporation) was used to stamp a ring shape between the two electrodes to act as a sample solution well. The ring was designed such that a few millimeters of gold electrode could be uncovered within the ring. PDMS was cured at 75°C for 1 hour in a convective oven. The silver tipped gold electrode (cathode) was modified to form a silver chloride (AgCl) layer by electrolysis, using 1.5 V-DC voltage for 3 min in 1 M HCl solution [28].

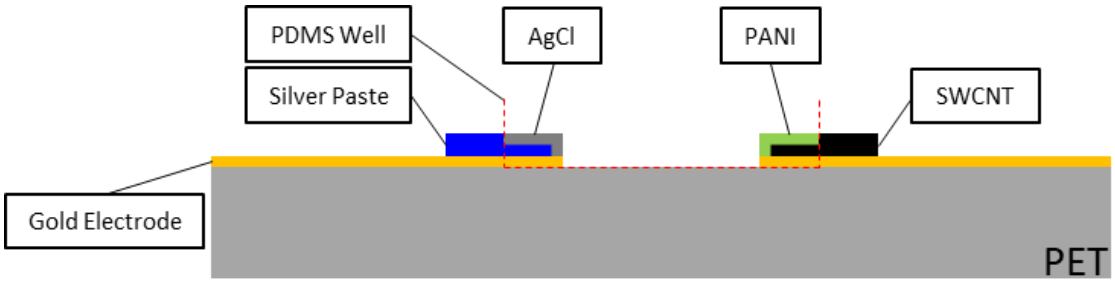

Fig. 4.1. pH sensor fabrication schematic.

Three layers of SWCNT, 5 mg/ml suspended in 1% sodium dodecyl sulfate (SDS) solution, were deposited onto the end of the other electrode (anode) with a Rotring Rapidograph Capillary Pen. Deposition of each layer SWCNTs was manually done over a hotplate at 100^{o}C followed by 10 min incubation. Polyaniline (5 mg/ml PANI,

emeraldine salt, Sigma-Aldrich Co, LLC.) suspended in 1% SDS was deposited on top of the SWCNT electrode using two 1 μl drops, followed by curing at in a convective oven at 120°C for 1 hour [28]. For electrical measurement 30 AWG wire was attached onto each electrode using a silver epoxy and baked for 45 minutes at 75^{o}C. The electrode regions were then wrapped with PET film to prevent any foreign elements from interfering with the sensor other than the sampling region.

4.1.2 *Humidity Sensor*

MWCNT powder was prepared in a 1% SDS solution with deionized (DI) water, to a concentration of 5 mg/ml. The MWCNT solution was sonicated for 20 minutes, with a water medium, to consistently disperse the nanotubes. Kimtech Delicate Task Wipes tissue paper was lightly wrinkled. The MWCNT solution was deposited onto the paper by immersing the tissue into the solution. Once the tissue paper was visibly saturated with MWCNT solution, it was dried in a convective oven at 60°C for 3~5 minutes. The MWCNTs were now evenly distributed and bound to the cellulose fibers of tissue paper after evaporation of the fluid. The tissue paper was then cut into a 20 x 3 mm sensor, with the sensing region identified as the central 10 x 3 mm area, leaving room to mount electrical wires. This size of the sensing area was based on a water absorption test, identified during prior research undertaken in the Nanomanufacturing Laboratory at University of Washington. For electrical transmission 30 AWG wire was attached onto each side of the sensor using a silver epoxy and baked for 45 minutes at 75^{o}C. The sensor was covered with a Teflon sheet, only leaving the 10 x 3 mm sensing region exposed [29].

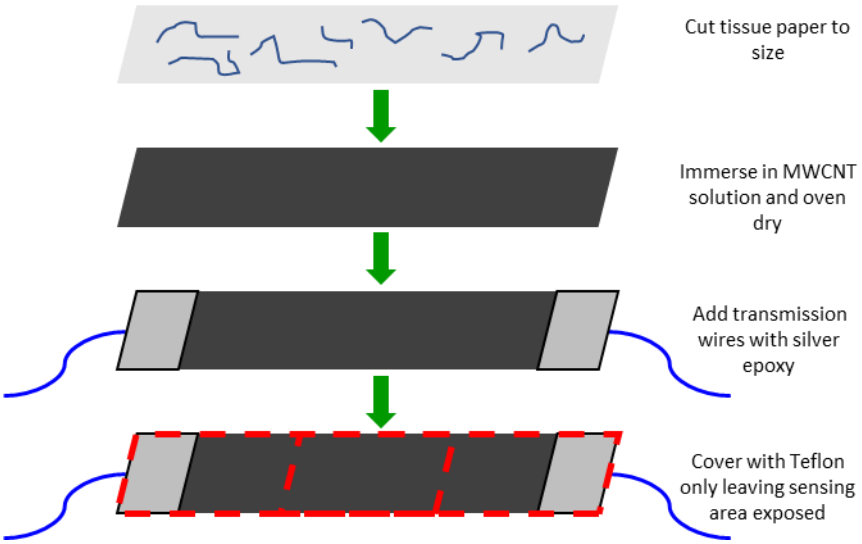

Fig. 4.2. Humidity sensor fabrication schematic.

4.1.3 *Temperature Sensor*

Except for its final packaging, fabrication of the temperature sensor was procedurally identical to that of a humidity sensor. After mounting the electrical wires, the sensor was completely sealed using a primary layer of 3M scotch tape and a secondary layer of Teflon tape, which ensured no moisture entered the sensing region.

Fig. 4.3. Temperature sensor partial fabrication schematic.

4.1.4 *Sodium Chloride Resistive Sensor*

The NaCl resistive sensor was housed on a PET substrate approximately 10 x 10 mm in size. 100 nM gold (Au) wires were cut into two approximately 15 mm in length pieces to serve as the sensing electrodes. The Au wires were twisted and connected onto 30 AWG wires for transmission of the electrical signal. The joint region was fastened

onto the PET substrate by using a silver epoxy and baked for 45 minutes at 75°C in a convection oven. To ensure uniformity in the sensing electrodes, they were each trimmed to ensure the sensing region (length) was equal. A thin layer of PDMS was then applied over the entire PET substrate. In the electrical connection, only the gold electrodes were protruded from the substrate. The PDMS coating must completely cover to protect the non-sensing regions from water. The sensor was subsequently cured at 75°C for 1 hour in a convective oven.

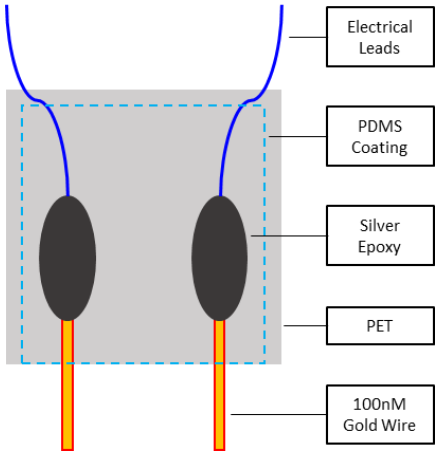

Fig. 4.4. Sodium chloride sensor fabrication schematic.

4.2 Sensor Casing Design

For easy use and wearable comfort, the sensors had to be housed on a single platform. The pH and NaCl sensors had to maintain contact with sweat molecules, while the humidity sensor must be guarded from any liquid saturation and vented to avoid excessive swelling. The temperature sensor was designed to transfer the temperature through conduction. A 100 μm thick film of PET was used as the substrate to house the four sensors, with laser cut slots to expose the transducing region (see Fig. 4.5). The pH and NaCl sensor slots were filled with single ply tissue paper to aid in wicking and

maintaining moisture at the transducer. The humidity sensor was positioned to allow for venting, as trapped water molecules could saturate the CPC and cause extreme changes in resistivity. The temperature sensor was firmly fastened onto the PET film to minimize the air gap and maximize conduction. Cables from each of the sensors ran over the PET layer and connected directly to the Arduino. The cable length was kept at minimum to reduce unnecessary electrical noise. The sensor casing remained flexible, owing to the thin profile and free regions between the sensors.

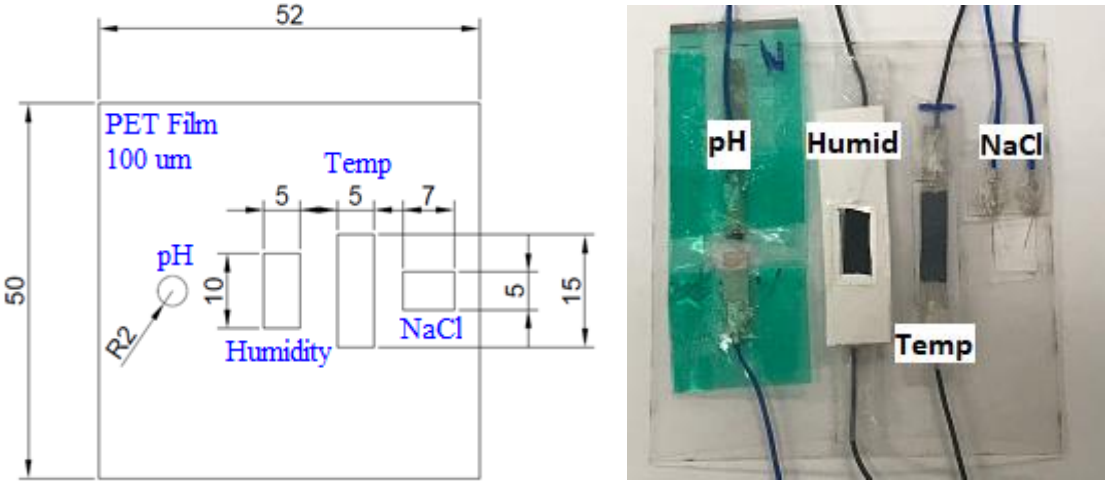

(a) (b)

Fig. 4.5. (a) Sensor casing design. (b) Actual sensor casing with sensors mounted.

4.3 Arduino Setup and Sensor Circuitry

The Elegoo Uno R3 arduino was used to detect and process the signals output by each of the four biosensors and the reference humidity and temperature sensors. The signal from each biosensor was measured in terms of a voltage potential using custom circuitry. To reduce noise and erroneous signals, the arduino was coded (refer to

Appendix A for full code) to record the average from 70 voltage readings per second, per analogue channel. Circuitry specifications for each biosensor are as follows;

pH Sensor: the pH sensor was an ion transducer and did not require a bias potential to detect the biological sample (sweat). The sensor was connected between analogue input A0 and ground (refer to Fig. 4.6), to measure a potential in volts in one second intervals.

Humidity and Temperature Sensors: were resistive CPC sensors that required a voltage input in order to establish a potential output with respect to the sample element. Both sensors were connected in series with a 100 kΩ reference resistor to mimic a *voltage divider* type circuit. The magnitude of the reference resistor was selected to be within a magnitude of ±50% as compared to the biosensor, with the initial resistance of the biosensor established under normal laboratory conditions (~25^{o}C and ~30-40% humidity). With the temperature and humidity sensors in series with the reference resistors, an output signal in volts, was measured between biosensors and ground, through channels A1 and A2 (refer to Fig. 4.6) in one second intervals.

Sodium Chloride Sensor: Similar to the temperature and humidity sensors, the NaCl sensor required an input voltage bias to establish a potential output. However, as the sensor was prone to oxidation through electrolysis when charged between a sample, a pulse input was created to lower the rate of sensor degradation. Channel D7 provided a 5 V pulse with a period of 35 seconds (5 on / 30 off) to drive a relay switch operating a 1.61 V DC (AA battery) supply. This 1.61 V DC input was connected in series with a 1 MΩ reference resistor and the NaCl biosensor (refer to Fig. 4.6). An output potential was

then measured between the biosensor and analogue channel A3, for a 5 second period every 30 seconds.

Reference Temperature and Humidity Sensor: DHT21 AM2301 Digital Temperature Humidity Sensor Module was used as the reference sensor during experimentation. The sensor provided a digital output through channel D8 (refer to Fig. 4.6) every one second.

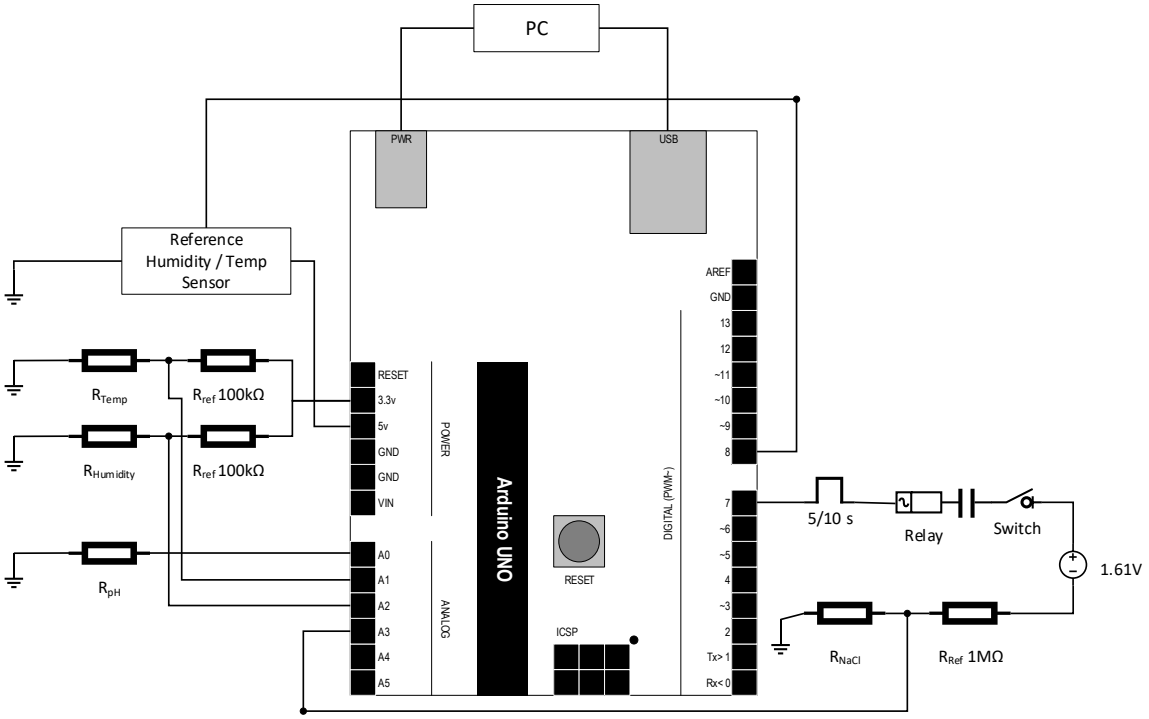

Fig. 4.6. Arduino sensor circuitry.

4.4 EXPERIMENTAL METHOD

The experimental method involved the initial calibration of each of the four sensors and then a sweat simulation test with all sensors simultaneously within the sensor housing. Each of the methods are as follows;

pH Sensor Calibration

1. pH base 4, 7, and 10 solutions were mixed with NaCl to 150 mM concentration.
2. 30 µl of 150 mM samples were placed on the pH sensor and cycled between solutions 4 to 10 and 10 to 4. Results were recorded.
3. 30 µl of 150 mM samples were placed on the pH sensor and cycled between solutions 4 to 7, with deionized water used to clean the sensor between each sample. Results were recorded.
4. pH 4 was mixed with NaCl to 150, 105 and 50 mM concentrations. 30 µl samples were placed on the pH sensor and cycled between each of the concentrations. Results were recorded.

Humidity Sensor Calibration

1. Humidity sensor, reference sensor and arduino were placed inside the humidity chamber.
2. 10ml of boiled water was placed in a glass beaker.
3. Humidity recording was initialized and the beaker was placed inside the humidity chamber. Recording continued until the reference sensor registered 100% humidity.
4. Test was repeated 5 times.

Temperature Sensor Calibration

1. Temperature sensor and reference sensor were placed on the hot plate.
2. Recording was initialized and hot plate temperature was increased in increments of 3^{o}C from 30^{o}C to 45^{o}C.
3. Test was repeated 5 times.

NaCl Sensor Calibration

1. NaCl solutions with a pH 4 base were mixed at 150, 105, 50 and 25mM concentrations.
2. 30 µl samples were placed on the NaCl sensor and cycled between each concentration. Deionized water used to clean the sensor between each sample. Results were recorded.

Sweat Simulation Test

1. 80 x 20 mm piece of tissue paper was saturated with 30 µl of 200 mM NaCl solution with a pH 4 or Phosphate Buffered Saline (PBS; 200 mM NaCl) base. As the pH sensor is sensitive to any ionic conductivity changes i.e. NaCl levels, the sample concentration was maintained at 200 mM (greater than max human sweat range) so only deviations in pH are detected. See Fig. 4.7 for setup schematic and image.
2. The tissue paper was placed over a hot plate. See Fig. 4.7 for layout.
3. The biosensors and reference sensor were placed on top on the wet tissue paper. Arduino recording was initialized.
4. Heater increased to 40^{o}C with continued recording until the reference sensor cycled back to the initial humidity reading registered during Step 3.
5. Test was repeated 5 times with pH 4 and PBS samples.

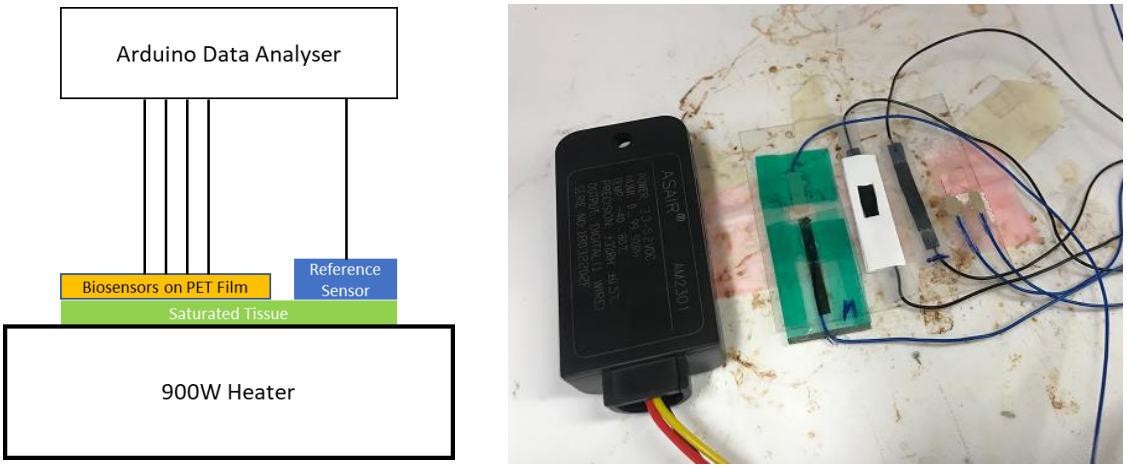

(a) (b)

Fig. 4.7. (a) Sweat simulation test on heated plate setup schematic. (b) Actual experimental setup.

Chapter 5. RESULTS AND DISCUSSIONS

The pH sensor's performance to monitor real time variations in pH was tested by cyclically sampling 150 mM NaCl solution at pH 4, 7 and 10 (refer to Fig. 5.1 (a)). A distinct change in potential was noted when varying the pH, while highly acidic or basic samples appeared to affect the sensors ability to accurately detect more neutral pH levels. A ~20% variance in potential was evident with pH 7 from when it was preceded by a sample of pH 4 versus pH 10. This variance could most likely be countered by increasing the hold time of the sample and more gradually increasing / decreasing the pH base to allow the sensor to stabilize.

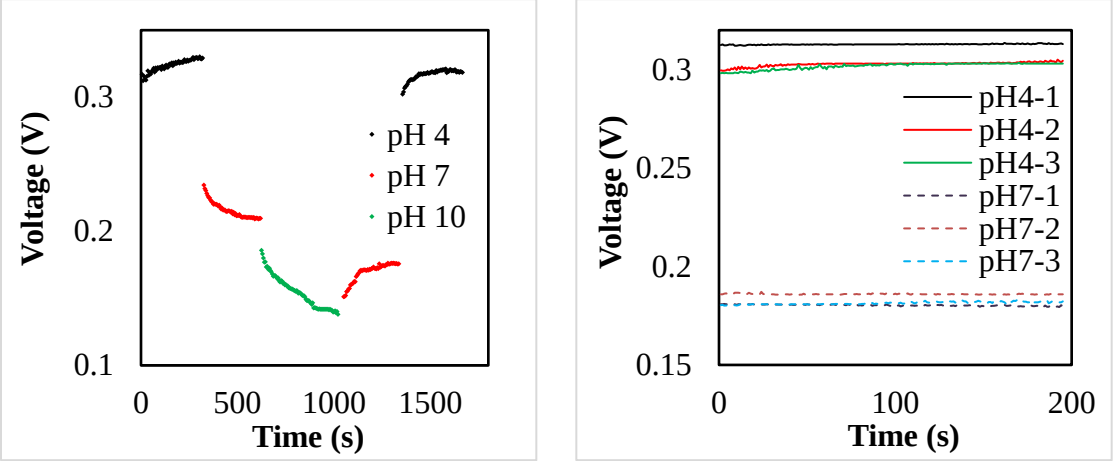

(a) (b)

Fig. 5.1. (a) Cyclic sampling of 150mM NaCl solution at pH 4, 7 and 10. (b) Calibration data for 150mM NaCl solution at pH 4 and 7.

The sensor was calibrated within the simulated sweat pH range of 4 to 7. Fig. 5.1 (b) shows consistency between each test and a definitive difference in potential magnitude between pH 4 (~0.305 V) and pH 7 (~0.182 V). The pH sensor sensitivity was

determined to be 41.1 mV/pH Unit, using this data. The Nernst equation, shown by Eqn. 5.3, evaluates the potential of an electrochemical cell under non-standard conditions.

$$\varepsilon = \varepsilon^o - \frac{RT}{nF}\ln Q \xrightarrow{25^oC} \varepsilon = \varepsilon^o - \frac{0.0592}{n}\log Q \tag{5.3}$$

, where ε is the cell potential, ε^o is the standard cell potential, R is the gas constant (8.314 J/Kmol), T is temperature, n is the number of electrons transferred, F is Faraday's constant (96,500 C/mol) and Q is the reaction quotient/solution concentration. Therefore, the theoretical Nernst slope was 59.2 mV/pH unit at 25°C. A ~30% variance was evident between the theoretical and experimental slope. This difference could be attributed to the high concentration of NaCl in the pH solution and uneven dispersion of CNTs on the sensing electrode. Calibration curves from Fig. 5.1 exhibit a similar trend to data from Rahimi et al. (Fig. 1.1), further validating the performance of the pH sensor. To discover if the pH sensor was sensitive to variations in NaCl, a calibration test was conducted with varying NaCl concentrations while maintaining a pH of 4 (refer to Fig. 5.2).

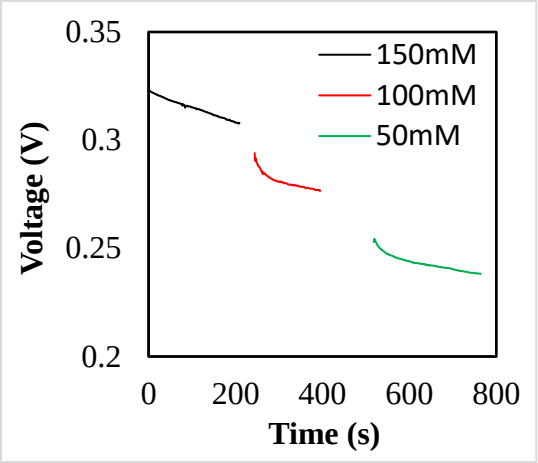

Fig. 5.2. (a) NaCl concentration varied between 150, 100 and 50 mM at pH 4.

Varying NaCl concentration showed a significant difference in potential, which would corrupt readings from changes in pH only. This result is indicative of the dominating effect of NaCl concentrations on the accuracy of the pH sensor. Thus, the sample concentration from the sweat simulation test was maintained at 200 mM (greater than max human sweat range) so only deviations in pH were detected.

The humidity sensor calibration curve was produced by plotting the resistance measured at the CPC sensor against the humidity registered by the reference sensor. A linear trend with a positive gradient was evident (shown in Fig. 5.3) between 45 to 80% humidity. This correlated with the working principle that increasing the humidity increased the resistance. The line of regression from the calibration curve is described by Eqn. 5.4, where H is humidity and r_{nh} the normalized resistance. Humidity sensor data collected from the sweat simulation test was expressed by using this linear line of regression.

$$H = 89.84 r_{nh} - 40.1 \qquad R^2 = 0.98 \tag{5.4}$$

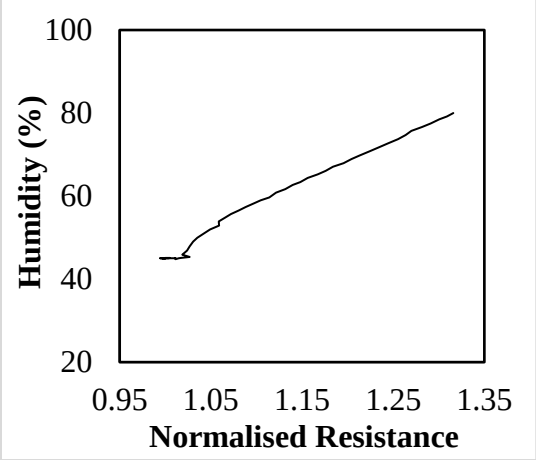

Fig. 5.3. Humidity sensor calibration plot.

The temperature sensor calibration curve was produced by plotting the resistance measured at the CPC sensor against the temperature registered by the reference sensor. A linear trend with a negative gradient was evident (shown in Fig. 5.4 (a)), which correlated with the working principle that increasing the temperature results in decreasing sensor resistivity. Temperature sensor data collected from the sweat simulation test was expressed by using the linear line of regression fitted to the data points from Fig. 5.4 (a). Initial results from the sweat simulation test indicated data that opposed information from the reference sensor. Water molecules interacting with the temperature CPC would result in behavior similar to the humidity sensor and explain the opposing trend. An insufficient seal and porous nature of the 3M scotch tape was suspected as the cause for allowing water molecule interaction. Teflon tape was now applied over the 3M scotch tape to provide a non-porous seal prior to retesting the sensor. However, the results still indicated an opposing trend that could indicate water infiltration into the MWCNT and the potential swelling of cellulose fibers [30]. This speculation was checked by recalibrating the sensor (now with a Teflon layer) to redefine the data collected from the sweat simulation test. Fig. 5.4 (b) shows the recalibrated sensor data with a linear positive slope, defined by Eqn. , where T is temperature and r_{nt} the normalized resistance.

$$T = 142.34 r_{nt} - 117.11 \qquad R^2 = 0.90 \tag{5.5}$$

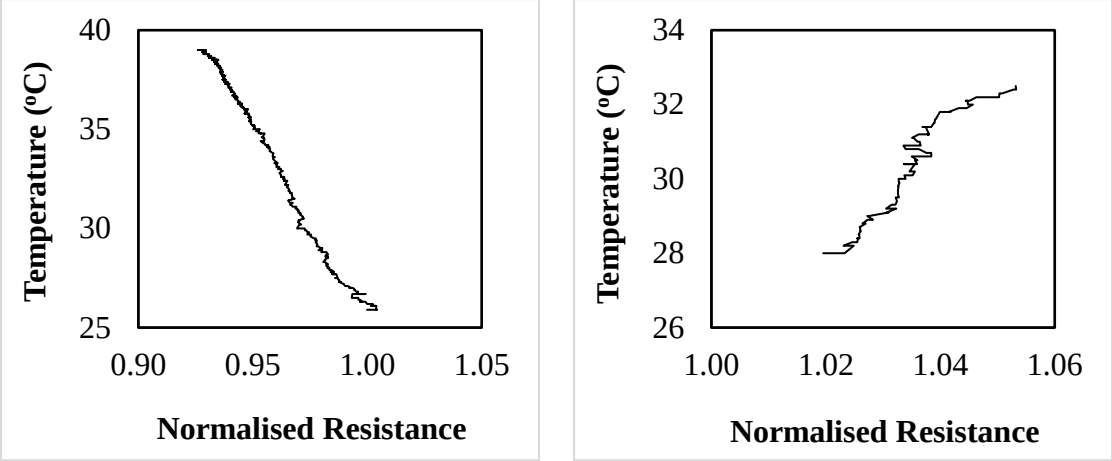

(a) (b)

Fig. 5.4. (a) Temperature sensor calibration without Teflon outer layer. (b) Temperature calibration with Teflon outer layer.

The NaCl sensor calibration results showed a negative linear trend, with voltage decreasing as the NaCl concentration increased. The result agreed with the expected outcome as the voltage decrease indicated a decrease in the resistance of the sample, with respect to the arduino circuitry used. The higher NaCl concentrations decreased the resistance. Fig. 5.5 (a) shows the change in voltage with respect to varying NaCl concentration in pH 4 solution. The average potential values at each concentration level was used to derive the plot shown Fig. 5.5 (b), where the sensitivity of the sensor was determined to be 1.34 mV/mM.

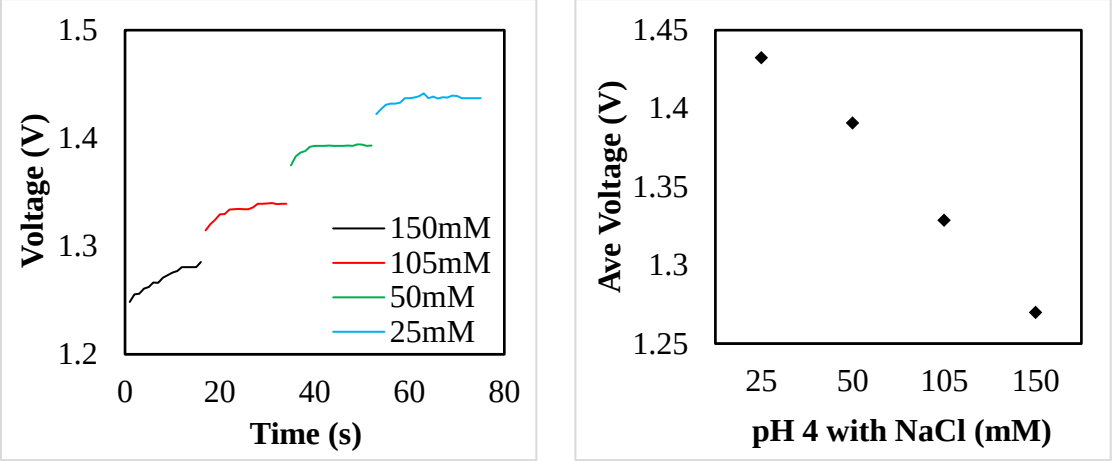

(a) (b)

Fig. 5.5. (a) NaCl sensor calibration at varying NaCl concentration levels at pH 4. (b) Average potential from NaCl sensor calibration.

5.1 Sweat Simulation Test

Sweat simulation test results for the pH, NaCl, humidity and temperature sensors are shown in Fig. 5.7. The pH sensor data was adjusted with respect to the calibration curves and translated to pH units from voltage output. The adjusted pH sensor results showed stability at pH 3.8, a 5% variance from the expected pH 4. The loss of data points after the 1000 second mark was due to the lack of contact with the sample fluid due to evaporation. To further evaluate the impact of NaCl concentration on the pH sensor, a PBS sample at 200 mM NaCl and pH 7.4 was tested. PBS contains chemical (NaCl, K^+, Phosphate etc.) constituents similar to blood and is therefore useful in analyzing the dominance of NaCl amongst other chemical elements. Fig. 5.6 shows the pH sensor stabilizing at pH 7.6, a ~3% variance from the expected pH 7.4. The dominant effect of sodium chloride is validated, as the pH sensor is calibrated with respect to NaCl concentrations and not the other chemical elements. If the other chemical constituents

had an impact on the pH sensor's performance, the accuracy of the sensor would have been affected more severely.

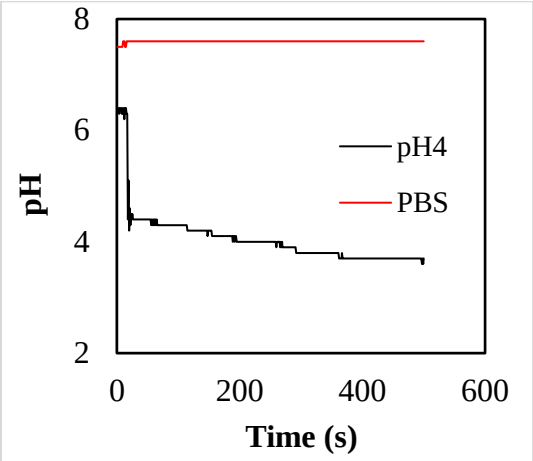

Fig. 5.6. pH sensor results from pH 4 and PBS samples at 200 mM of NaCl.

The NaCl sensor data was converted to concentration units from voltage. The sensor stabilized at ~180 mM, which was 20 mM below the expected 200 mM sample concentration. This 10% error margin and general instability was attributed to lack of contact between the sensor's gold prongs and the sample. Sensor design must be revised to increase transducer contact area, thus ensuring sufficient interaction with the sample, reducing instability. The loss of data points after the 500 second mark indicated the loss of the electrical contact with the sample due to evaporation. The trend from the humidity sensor was similar to the reference sensor, but with considerable deviation in data as the humidity began to cycle down from 100%. This deviation was likely due to the difference in boundary conditions between the reference and humidity sensors. Although both sensors were arranged onto the wet tissue and hot plate, the humidity sensor had a very small air gap with sufficient venting to allow steady evaporation. However, the reference sensor laid flat on the wet tissue without adequate venting. This inadequacy in ventilation

was clear as the reference sensor held at 100% humidity for nearly 500 seconds longer than the humidity sensor. The humidity sensor showed good repeatability as cycled down to the initial humidity range at the end of the test. This suggests the resistivity of the CPC sensor should be proficient in capturing real time data.

The recalibrated temperature sensor data displayed a similar trend to the reference data, suggesting the potential water infiltration into the sensor. Application of the Teflon outer layer has trapped water molecules absorbed from pervious tests, causing a permanent change in the conductive behavior of the CNTs and cellulose fibers. The difference in magnitude between the reference and temperature sensor could be attributed to the thickness of sensor packaging and lack of contact between sensor surface the hot plate.

The sensor casing design was determined to be suitable but not ideal for housing this variety of sensors. The pH, temperature and NaCl sensors work most effectively in contact with the sample / surface, while the humidity sensor required a small air gap and must be guarded from any with liquids. This case was effective in ensuring contact between the sample and the pH, temperature and NaCl sensors. However, the profile was so thin that water molecules could come into direct contact with the humidity sensor. Any application of pressure or movement of the casing during testing would often result in the humidity sensor becoming lightly saturated and void any collected data. Furthermore, the casing was observed to suffer from lack of ventilation (slowed evaporation rate), which would potentially affect real time sweat monitoring by mixing ‘old’ and ‘new’ sweat during human trials. A revised design should include a staggered thickness profile on a flexible substrate i.e. PDMS, with multiple ventilation slots around the sensing region.

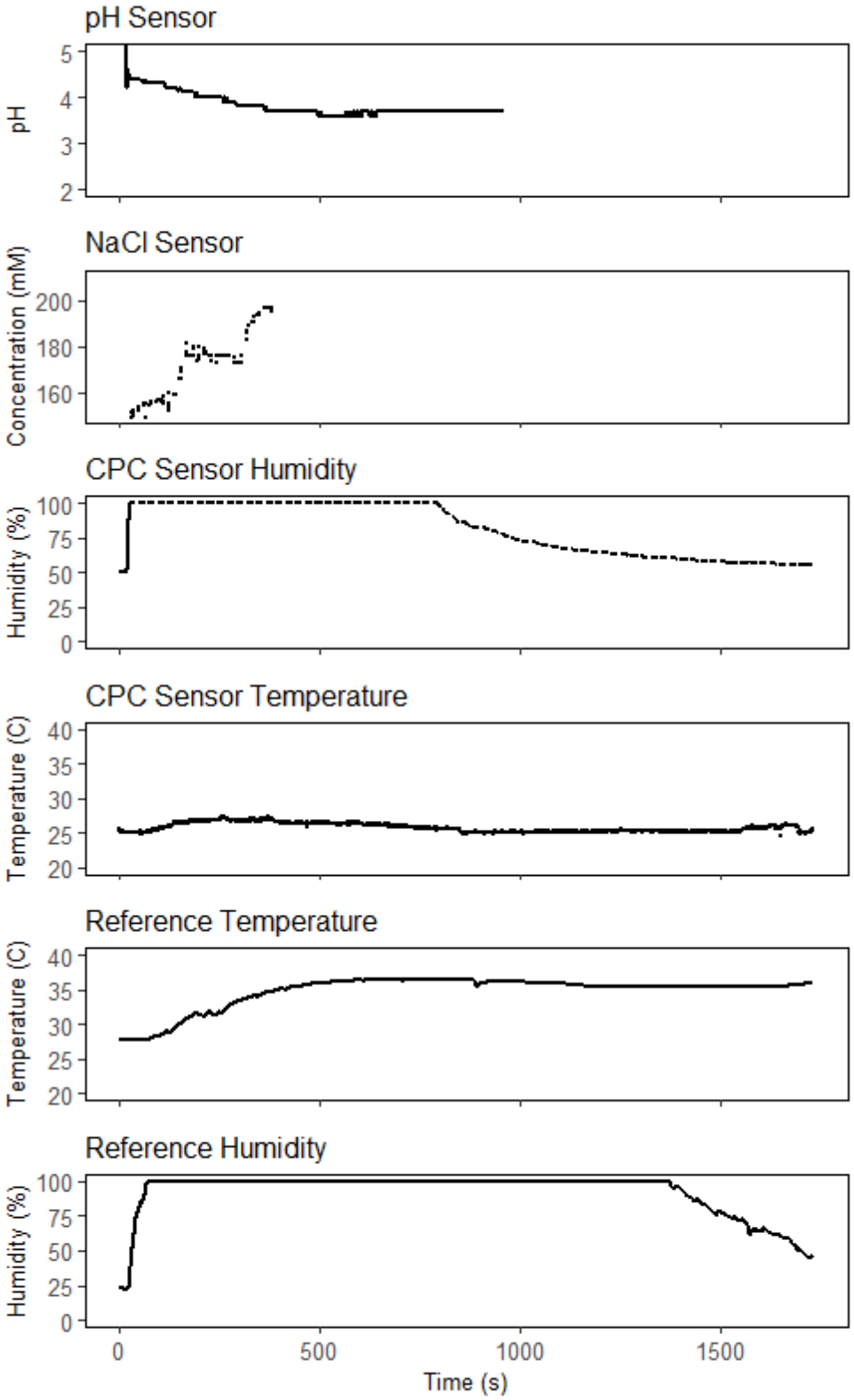

Fig. 5.7. Sweat simulation test sensor results

Chapter 6. CONCLUSIONS

A multiplexing wearable sweat sensor was developed using single and multi-walled carbon nanotubes, while negating the need for complex microfabrication techniques. The pH, temperature, humidity and NaCl sensors were developed without cleanroom environment. The pH, temperature and humidity sensors utilized single and multi-walled carbon nanotubes as the sensor transducer. The pH sensor proved effective in detecting real time changes in pH, but was affected by NaCl concentrations. The fluctuations in NaCl had to be controlled through design, by using a tissue pad to stabilize the concentration level to the maximum physiological range. The humidity sensor was highly sensitive to changes in humidity and showed good repeatability once evaporation and diffusion issues were addressed. The temperature sensor performed well during calibration, but suffered from sealing issues that trapped water molecules (during testing), subsequently swelling cellulose fibers. The NaCl sensor accurately detected changes in concentration in a pH solution. Sensor packaging design was adequate but not ideal for integration of the various sensors. Further design iterations were necessary to separate the dry and wet type sensors, while specifically integrating increased ventilation for the humidity sensor and ensuring contact between the temperature sensor and sample.

The simulated sweat test demonstrated that the multiplexing sensor was capable of real time sweat monitoring. Design optimizations and sensor fabrication refinements are required to increase the accuracy, sensitivity and durability of the multiplexing device, prior to human trials. With further optimization of the sensing platform, a human subject test will be conducted. The sensing platform will facilitate a simple integrated platform for sweat analysis, beneficial to various disease diagnosis and health monitoring.

BIBLIOGRAPHY

[1] D. R. Thevenot, K. Toth, R. A. Durst, and G. S. Wilson, "Electrochemical Biosensors: Recommended Definitions and Classification," *Int. UNION PURE Appl. Chem.*, vol. 71, no. 20, pp. 655–657, 1999.

[2] H. C. Koydemir and A. Ozcan, "Wearable and Implantable Sensors for Biomedical Applications," *Annu. Rev. Anal. Chem.*, vol. 11, no. 1, pp. 127–146, 2018.

[3] A. M. A. Mcwilliams, "Devices : Markets Chapter 1 : Introduction," no. April, pp. 0–7, 2019.

[4] M. M. Bellah, S. M. Christensen, and S. M. Iqbal, "Nanostructures for Medical Diagnostics," *J. Nanomater.*, vol. 2012, no. November 2016, pp. 1–21, 2012.

[5] A. Vaseashta and D. Dimova-Malinovska, "Nanostructured and nanoscale devices, sensors and detectors," *Sci. Technol. Adv. Mater.*, vol. 6, no. 3-4 SPEC. ISS., pp. 312–318, 2005.

[6] F. Du, L. Zhu, and L. Dai, "Carbon nanotube-based electrochemical biosensors," *Biosens. Based Nanomater. Nanodevices*, no. ii, pp. 273–293, 2017.

[7] B. Schazmann *et al.*, "A wearable electrochemical sensor for the real-time measurement of sweat sodium concentration," *Anal. Methods*, vol. 2, no. 4, pp. 342–348, 2010.

[8] S. Elmståhl and L. Winge, "Increased Sweat Sodium Concentration in Patients with Alzheimer's Disease," *Dement. Geriatr. Cogn. Disord.*, vol. 4, no. 1, pp. 50–53, 2007.

[9] E. Pinilla-Gil, "Wearable electrochemical sensors: innovative tools for the emerging mobile health ecosystem," *J. Appl. Bioanal.*, vol. 1, no. 3, pp. 68–71,

2015.

[10] K. Wilke, A. Martin, L. Terstegen, and S. S. Biel, “A short history of sweat gland biology,” *Int. J. Cosmet. Sci.*, vol. 29, no. 3, pp. 169–179, 2007.

[11] S. K. Hall, D. E. Stableforth, and A. Green, “Sweat sodium and chloride concentrations - Essential criteria for the diagnosis of cystic fibrosis in adults,” *Ann. Clin. Biochem.*, vol. 27, no. 4, pp. 318–320, 1990.

[12] W. Gao *et al.*, “Fully integrated wearable sensor arrays for multiplexed in situ perspiration analysis,” *Nature*, vol. 529, no. 7587, pp. 509–514, 2016.

[13] H. Y. Y. Nyein *et al.*, “A Wearable Microfluidic Sensing Patch for Dynamic Sweat Secretion Analysis,” *ACS Sensors*, vol. 3, no. 5, pp. 944–952, 2018.

[14] M. Kaempgen and S. Roth, “Transparent and flexible carbon nanotube/polyaniline pH sensors,” *J. Electroanal. Chem.*, vol. 586, no. 1, pp. 72–76, 2005.

[15] V. F. Curto *et al.*, “Sensors and Actuators B : Chemical Real-time sweat pH monitoring based on a wearable chemical barcode micro-fluidic platform incorporating ionic liquids,” *Sensors Actuators B. Chem.*, vol. 171–172, pp. 1327–1334, 2012.

[16] M. J. Patterson, S. D. R. Galloway, and M. A. Nimmo, “Variations in regional sweat composition in normal human males,” no. August, 2000.

[17] R. Rahimi *et al.*, “A low-cost flexible pH sensor array for wound assessment,” *Sensors Actuators, B Chem.*, vol. 229, pp. 609–617, 2016.

[18] S. J. Montain, L. A. Stephenson, S. N. Cheuvront, H. C. Lukaski, and A. J. Young, “Sweat Electrolyte and Mineral Responses during 7 h of Exercise-Heat Stress,” *Med. Sci. Sport. Exerc.*, vol. 38, no. Suppl 1, p. S29, 2006.

[19] S. Sugama *et al.*, “A Soft, Wearable Microfluidic Device for the Capture, Storage, and Colorimetric Sensing of Sweat,” *Sci T ransl Med Sci*, vol. 8, no. 366, pp. 39–46, 2017.

[20] S. Anastasova *et al.*, “Corrigendum to ‘A wearable multisensing patch for continuous sweat monitoring’ (Biosensors and Bioelectronics (2016) 93 (139–145) (S0956566316309198) (10.1016/j.bios.2016.09.038)),” *Biosens. Bioelectron.*, vol. 94, no. June 2016, p. 730, 2017.

[21] Y. K. Axelrod and M. N. Diringer, “Temperature Management in Acute Neurologic Disorders,” *Neurol. Clin.*, vol. 26, no. 2, pp. 585–603, 2008.

[22] A. Aqel, K. M. M. A. El-Nour, R. A. A. Ammar, and A. Al-Warthan, “Carbon nanotubes, science and technology part (I) structure, synthesis and characterisation,” *Arab. J. Chem.*, vol. 5, no. 1, pp. 1–23, 2012.

[23] T. S. Li, C. H. Lee, and M. F. Lin, “Electron transport in double-walled carbon nanotubes,” *Eur. Phys. J. B*, vol. 60, no. 1, pp. 45–50, 2007.

[24] M. Cen-Puc, A. I. Oliva-Avilés, and F. Avilés, “Thermoresistive mechanisms of carbon nanotube/polymer composites,” *Phys. E Low-Dimensional Syst. Nanostructures*, vol. 95, no. September 2017, pp. 41–50, 2018.

[25] M. Dimaki, P. Bøggild, and W. Svendsen, “Temperature response of carbon nanotube networks,” *J. Phys. Conf. Ser.*, vol. 61, no. 1, pp. 247–251, 2007.

[26] J. W. Bennett, T. Thio, H. Hiura, H. J. Lezec, T. W. Ebbesen, and H. F. Ghaemi, “Electrical conductivity of individual carbon nanotubes,” *Nature*, vol. 382, no. 6586, pp. 54–56, 2003.

[27] D. H. Choi, Y. Li, G. R. Cutting, and P. C. Searson, “A wearable potentiometric

sensor with integrated salt bridge for sweat chloride measurement," *Sensors Actuators, B Chem.*, vol. 250, pp. 673–678, 2017.

[28] S. J. Kahng *et al.*, "Nanoink bridge-induced capillary pen printing for chemical sensors," *Nanotechnology*, vol. 29, no. 33, 2018.

[29] J. Zhang *et al.*, "Fracture-Induced Mechanoelectrical Sensitivities of Paper-Based Nanocomposites," *Adv. Mater. Technol.*, vol. 3, no. 3, pp. 1–7, 2018.

[30] A. Zahab, L. Spina, P. Poncharal, and C. Marlière, "Water-vapor effect on the electrical conductivity of a single-walled carbon nanotube mat," *Phys. Rev. B - Condens. Matter Mater. Phys.*, vol. 62, no. 15, pp. 10000–10003, 2000.

APPENDIX A

Arduino Code – Quad Sensors

```
#include <SD.h>
#include <SPI.h>
#include <DHT.h>
#define DHTPIN 2
#define DHTTYPE DHT21

DHT dht(DHTPIN, DHTTYPE);

const int chipSelect = 4;

unsigned long previousTimePulse = 0;
boolean high = true; //true if next pulse is high, false if next pulse
is low
unsigned long previousTimePrint = 0;

long waitAfterHigh = 5000; //time to wait after high pulse
long waitAfterLow = 20000; //time to wait after low pulse
long printInterval = 1000; //time between printing

void setup() {
    Serial.begin(9600);
    SD.begin(4);
    dht.begin();
    pinMode(8, OUTPUT);
    pinMode(7, OUTPUT);
}

void loop() {

  // Reading temperature or humidity takes about 250 milliseconds
  // Sensor readings may also be up to 2 seconds 'old' (its a very slow
sensor)

 float h = dht.readHumidity();
 float t = dht.readTemperature();

 //get the current time
 unsigned long currentTimePulse = millis();

 // 5V Pulse from Digital Pin 7
 if (high && currentTimePulse - previousTimePulse >= waitAfterLow) {
   digitalWrite(7, HIGH);
   previousTimePulse = millis();
   high = !high;
 } else if (!high && currentTimePulse - previousTimePulse >=
waitAfterHigh) {
   digitalWrite(7, LOW);
   previousTimePulse = millis();
   high = !high;
 }
```

```
digitalWrite(8,HIGH);

// averaging

int j = 1;
float avgn0;
float volt0;
float k = 0;
float n = 0;

for (j = 1; j < 71; j++) {
    n = analogRead(A0);
    k = n + k;
}

avgn0 = k / 70;
volt0 = avgn0 * (0.0048876);

int i = 1;
float avgnt;
float voltt;
float kt = 0;
float nt = 0;

for (i = 1; i < 71; i++) {
    nt = analogRead(A1);
    kt = nt + kt;
}

avgnt = kt / 70;
voltt = avgnt * (0.0048876);

int l = 1;
float avgnh;
float volth;
float kh = 0;
float nh = 0;

for (l = 1; l < 71; l++) {
    nh = analogRead(A2);
    kh = nh + kh;
}

avgnh = kh / 70;
volth = avgnh * (0.0048876);

int m = 1;
float avgnr;
float voltr;
float kr = 0;
float nr = 0;

for (m = 1; m < 71; m++) {
    nr = analogRead(A3);
    kr = nr + kr;
}
```

```
avgnr = kr / 70;
voltr = avgnr * (0.0048876);

// Averaging of data points complete

File dataFile = SD.open("datalog.txt", FILE_WRITE);

unsigned long currentTimePrint = millis();
if (currentTimePrint - previousTimePrint >= printInterval) {
  previousTimePrint = currentTimePrint;

  Serial.print("REF Hum: ");
  Serial.print(h);
  Serial.print(" %\t");
  Serial.print("REF Temp: ");
  Serial.print(t);
  Serial.print(" C");
  Serial.print("\t pH: ");
  Serial.print(volt0,6);
  Serial.print(" V\t");
  Serial.print("\t Temp: ");
  Serial.print(voltt,6);
  Serial.print(" V");
  Serial.print("\t Humid: ");
  Serial.print(volth,6);
  Serial.print(" V");
  if (!high) {
    Serial.print("\t NaCl: ");
    Serial.print(voltr,6);
    Serial.print(" V");
  }
  Serial.println("");
}

if(dataFile){

    // LED will flash once if the value is less than 0
    if(volt0 < 0){
        digitalWrite(8,LOW);
    }

    dataFile.print(volt0);
    dataFile.println();

    dataFile.close();

    n = 0;
    k = 0;
    avgn0 = 0;
    volt0 = 0;

    nt = 0;
    kt = 0;
    avgnt = 0;
    voltt = 0;
```

```
            nh = 0;
            kh = 0;
            avgnh = 0;
            volth = 0;

            nr = 0;
            kr = 0;
            avgnr = 0;
            voltr = 0;
        }
    }
```